UCRL-JC-123378
PREPRINT

CONF-960772--8

Experimental and Modeling Studies of the Micro-Structures of Opposed Flow Diffusion Flames: Methane

A. M. Vincitore, N. Marinov, W. J. Pitz,
C. K. Westbrook, C. F. Melius, S. M. Senkan

This paper was prepared for submittal to the
Twenty-Sixth Symposium on Combustion
Napoli, Italy
July 28-August 2, 1996

February 1996

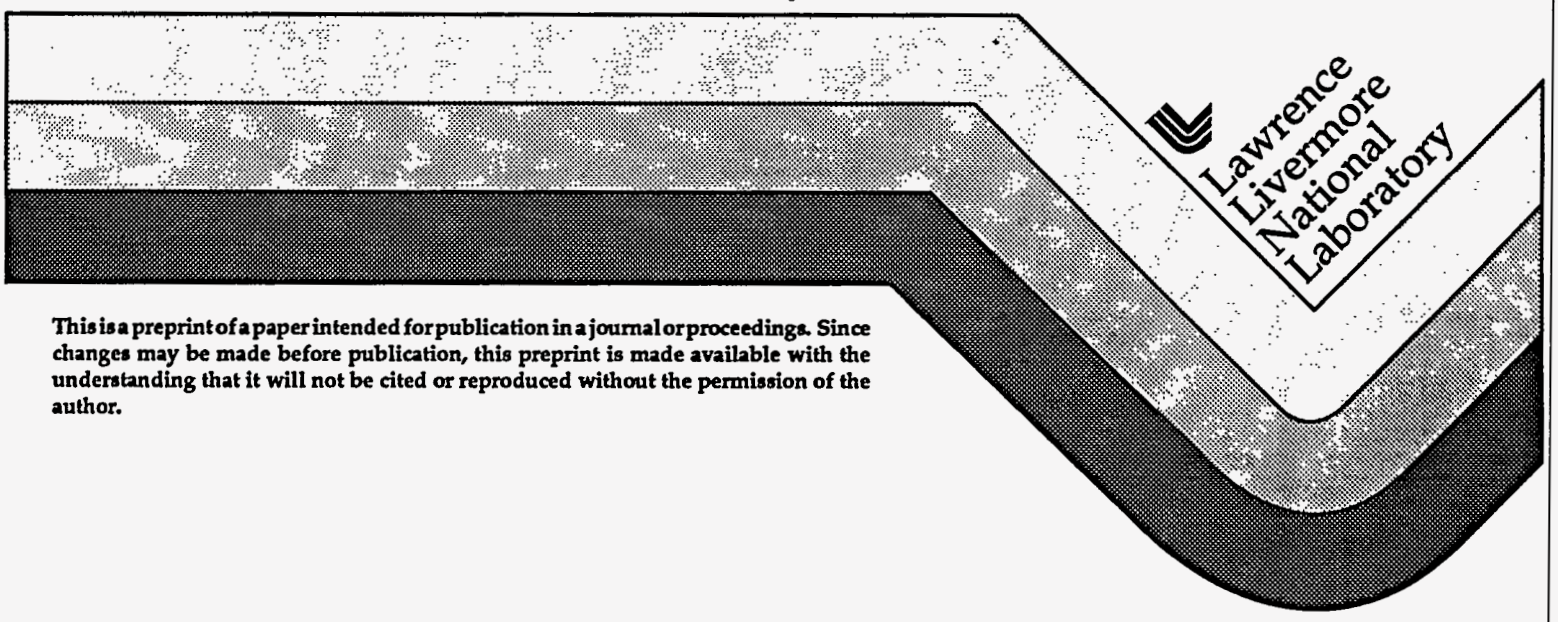

Experimental and Modeling Studies of the Micro-Structures of Opposed Flow Diffusion Flames : Methane

by

Antonio M. Vincitore[1], Nick Marinov[2], William J. Pitz[2], Charles K. Westbrook[2], Carl F. Melius[3], and Selim M. Senkan[*1]

[1] Department of Chemical Engineering
University of California
Los Angeles, CA 90095 USA

[2] Lawrence Livermore National Laboratory
Livermore, CA 94551 USA

[3] Combustion Research Facility
Sandia National Laboratories
Livermore, CA 94551 USA

January 15, 1996

Prepared for the Twenty-Sixth Symposium (International) on Combustion

Abstract = 133 words
Text = 3238 words
Figures = 1000 words (5 figures)
Tables = 200 words (1 table)
References = 624 words
Total = 4438 words (text + 1 table+ 5 figures)

Colloquium Topic Area = Soot and PAH, Flame Structure
Oral Presentation

* To whom correspondence should be addressed: Tel: (310) 206-4106, Fax: (310)206-4107, e.mail: senkan@seas.ucla.edu

Abstract

The micro-structure of an atmospheric pressure, opposed flow, methane diffusion flame has been studied using heated micro-probe sampling and chemical kinetic modeling. Mole fraction profiles of major products as well as trace aromatic, substituted aromatic, and polycyclic aromatic hydrocarbons (PAH up to $C_{16}H_{10}$, e.g. pyrene) were quantified by *direct* gas chromatography/mass spectrometry (GC/MS) analysis of samples withdrawn from within the flame without any pre-concentration. Mole fractions range from 0.8 to 1.0×10^{-7}. The experimental measurements are compared to results from a newly-developed chemical kinetic model that includes chemistry for the production and consumption of aromatics and PAH species. The model predictions are in reasonable agreement with the experimental data for the major species profiles and for the peak concentrations of many of the trace aromatics and PAH species.

Introduction

Combustion is the major source of energy production today, as well as being the principal contributor to air pollution. Over the recent years, a shift towards pollution prevention and minimization has been evident from the passing of legislature regulating the emission of pollutants formed as side products from various chemical processes [1]. As a first step in curtailing emissions, the effects of operating parameters on the formation and destruction of toxic compounds generated by combustion processes must be understood. This information is also needed to develop realistic, science based regulations and achievable pollution control technologies. The formation of polycyclic aromatic hydrocarbons (PAH) in combustion is of particular concern due to the carcinogenic potency of some isomers [2]. They are also believed to be precursors to soot, which has its own problems. Although PAH are formed at trace levels, they often represent the greatest health risk induced by combustion systems [3,4]. Therefore, the ultimate goal is to reduce these emissions by burner modifications or new technologies developed from a better understanding of the mechanisms of PAH formation.

Opposed flow flames of hydrocarbons, both in premixed and diffusion systems, have been extensively studied in the past with respect to soot, NO_x, and flame extinction [5,6,7]. In contrast,

the detailed chemical structures of counterflow diffusion flames, especially with regards to the formation of trace aromatic and PAH have received little attention. Tsuji and Yamaoka [8] measured species profiles across a methane-air counterflow diffusion flame, but did not measure aromatics and PAH. Computational analysis of opposed flow flames also has been limited with most studies using reduced reaction mechanisms to describe the major features of the flames [9,10]. However, the latter is due to the lack of detailed flame structure data. Recently Zhang *et al.* [11], studied a counterflow diffusion flame structure of methane using laser induced fluorescence (LIF). Although these investigators determined the total PAH levels, the concentration profiles of individual PAH were not provided. Distinction between individual PAH species is necessary in order to validate detailed chemical kinetic models. Health risk assessments also require some distinction between PAH species, because of the varying degree of toxicity and carcinogenicity of these pollutants [2].

In this paper, we report for the first time the micro-structure of an opposed jet diffusion flame of methane acquired through heated micro-probe sampling followed by *direct* gas analysis of aromatic and PAH species with an on-line GC/MS. Previous combustion studies have used sorbents to concentrate the aromatics and PAH's, which raises concerns about PAH recovery and gas sample contamination [3,4]. The mole fraction profiles for a total of 27 chemical species ranging from major to trace aromatic and PAH were determined. Experimental results are then compared to model predictions from a newly developed chemical kinetic mechanism. The key reaction pathways that lead to aromatics and PAH are discussed.

Experimental Set-up

An illustration of the experimental burner and sampling configuration is shown in Fig.1. A flat counterflow methane diffusion flame was stabilized between two opposed 1.0 inch ID burner ports and into which several layers of 100 mesh screens were imbedded. The screens were used to

generate plug velocity profiles resulting in a flat, stable flame. Flames were protected from the surrounding air by an argon gas shield. The shield gas also aided the cooling of hot combustion gases. The oxidizer stream composed of 20% O_2 (99% purity) and 80% Ar (99.99% purity) was introduced via the top burner port. The fuel stream, containing 75% CH_4 (99% purity) and 25% Ar, was introduced through the bottom port. All gases were then vented through the bottom port, that was water cooled [12]. Gas flows were regulated using high accuracy mass flow controllers (MKS, Burlington MA). Samples were withdrawn with a heated quartz microbe with a 100 μm orifice and transported through a silica lined, stainless steel transfer line to a GC/MS system. A quartz wool filter was placed inside the probe to trap soot particles. The entire sampling system was maintained at 300 °C to minimize the adsorption of large molecular weight PAH. The sampling line was tested for catalytic activity by passing unburned gas mixtures of various PAH species. No activity was detected.

Samples were then analyzed by a computer controlled gas chromatograph/mass spectrometer (Hewlett-Packard 5890/5971) using both capillary (0.25 mm x 60 m HP-5) and packed bed (Porapak N and Hayesep DB) columns. Major species were analyzed using the thermal conductivity detector (TCD). Some minor and all the trace species were analyzed using the mass spectrometer.

Species were identified by matching both the retention times (depending on the availability of the compound) and the mass spectral fingerprints (Wiley Mass Spectral Database). Species concentrations were then determined either by direct calibration standards (Matheson Gas), or by the use of mass spectral ionization cross section method [13]. The accuracy of latter has been reported to be within a factor of two, and was verified in the present studies. The accuracy of the mole fractions for major species determined by direct calibration is estimated to be ±15%.

Concentration profiles were generated by moving the entire burner assembly vertically up or

down with respect to the fixed sampling probe. Positional accuracy associated with the concentration and temperature measurements with respect to the burner port is estimated to be ± 0.25 mm. Temperature measurements were obtained with a silica coated, 0.15 mm Pt-13%Rh/Pt thermocouple. Temperature measurements reported were corrected for radiation losses.

Computational Model and Mechanism

The computational model used in this study is the Sandia laminar, one-dimensional, opposed-flow, diffusion flame code [14]. Thermochemical information was primarily obtained from the Chemkin thermodynamic database [15], Burcat and McBride [16] and, Stein and co-workers [17,18]. Unavailable thermodynamics for some species were estimated by group additivity and difference methods [19]. Thermochemical data obtained from sources other than the Chemkin thermodynamic database is presented elsewhere [20]. Lastly, the transport parameters were obtained from the Chemkin transport data base [21] and by the method described in Wang and Frenklach [22].

The compiled chemical kinetic mechanism was primarily framed around the Miller-Melius benzene formation submechanism [23] , Tsang's propane [24] and propene [25] chemical kinetic reviews, Pitz-Westbrook n-butane submechanism [26], and the Emdee-Brezinsky-Glassman toluene and benzene oxidation submechanisms [27]. The mechanism was extended to allow prediction of methyl-substituted aromatics, and for two to five fused-ring structures. The detailed chemical model used in this study consists of 685 reactions and 149 species. The full presentation and discussion of the chemical reactions and kinetic rates used in the detailed mechanism is presented in Marinov et al. [20].

Results and Discussion

Experimental conditions and the corresponding pre-reaction parameters are shown in Table 1. Experimental conditions selected allowed for a reproducible, stable, flat flame. Gas flowrates used

for the fuel and oxizider streams resulted in outlet burner velocities, at 298 K, of 13.16 cm/s and 16.12 cm/s, respectively. The strain rate for this methane flame was not measured because of the unavailability of suitable instrumentation. Consequently, it was calculated using the burner outlet velocities and the following equation [7];

$$K=\frac{-2u_o}{L}\left(1+\frac{u_f}{(-u_o)}\sqrt{\frac{\rho_f}{\rho_o}}\right)$$

where K, L, u_o,u_f, ρ_f, and ρ_o are the defined strain rate, burner separation distance, oxidizer outlet velocity, fuel outlet velocity, fuel stream density, and oxidizer stream density, respectively. This calculation led to the determination of a strain rate of 35 sec^{-1} at 298 K. The location of the stagnation plane was determined visually from the streamlines generated by silica particles introduced into the fuel stream from a particle generator. Based on the experimental conditions, the stagnation plane was located at 4 mm from the fuel burner port. The error associated with this measurement should be around ± 0.5 mm. The numerical model predicted that the stagnation plane is located at 5.0 mm which is close to the experimental measurement.

Flame Structure

Before discussing the results, a number features corresponding to the flame studied should be pointed out. Visually the flame exhibited blue, luminous yellow, and dark orange zones congruous to a diffusion flame, with the flame being positioned on the oxidizer side of the stagnation plane. Since oxygen is the limiting reactant, the methane has to diffuse across the stagnation plane into the oxidizer side. The blue zone, indicating the occurrence of reactions associated with stoichiometric flames, was approximately 1.5 mm thick. The luminous yellow and dark orange zones, indicating the

presence of higher molecular weight hydrocarbons and soot comprised a total thickness of 3.5 mm. However, the thickness of the sooting region relative to the luminous yellow zone was small. The total flame thickness was 5 to 5.5 mm. Flame thickness was recorded using a cathetometer with the probe tip serving as the reference point. Between the blue and luminous zones was a thin dark zone. During the screening experiments, the dark zone thickness was noted to directly change with the oxygen concentration in the oxidizer stream. Sampling was primarily focused on the fuel-rich side of the diffusion flame since the object of this study is to map the mole fraction profiles of trace aromatics and PAH. All concentration and temperature profiles presented were obtained at the center of the flame (r = 0), and represent the average of 3 separate experiments.

Low Molecular Weight Species

The measured and calculated CH_4, O_2, CO, CO_2, H_2, H_2O, and Ar mole fraction profiles along with the radiation-corrected temperature profile are shown in Fig. 2. As seen in this figure, the agreement between the model predictions and the experimental data is reasonable. The methane was consumed more slowly in the chemical kinetic model compared to the experiments. Significant O_2 penetration into the fuel rich portion of the flame, that was experimentally observed, is supported by the model. The concentration of CO increased as the fuel was consumed and exhibited a peak mole fraction of 0.033 at 4.5mm, followed by a sharp decrease with further increase in height above the fuel burner. The model predicted a 0.021 mole fraction of CO at its peak which is displaced to the right of the measured peak. This displacement is also seen in the H_2, H_2O and CO_2 profiles and is consistent with the slower consumption rate of CH_4 predicted by the model. The measured CO_2 and H_2O peak concentrations are in excellent agreement with the model. However, the model tends to overpredict the CO_2 concentrations near the oxidizer nozzle. The predicted maximum H_2 concentration is a factor of 2.5 below the measured maximum.

In Fig. 3, the measured and calculated C_2H_2, C_2H_4, C_2H_6, C_3H_4, C_4H_2,C_4H_4, and C_4H_6 mole fraction profiles are shown. No aliphatic hydrocarbons were detected beyond 6.5 mm from the fuel burner port. As seen in the figure, the experimental mole fractions of acetylene, ethylene and ethane decreased around 6.5mm, a result which is consistent with the flame structure studies by Tsuji and Yamoaka [8,28], and Zhang et al. [11]. Acetylene was the most abundant of the C_2 species, followed by ethylene, and ethane which is consistent with the modeling results. The measured acetylene concentration reached a maximum of 5000 ppm while the model underpredicted the maximum by a factor of four. Peak concentrations for ethylene and ethane were 1100 ppm and 800 ppm respectively and were well reproduced by the model. According to the model, the formation of the C_2 hydrocarbons occurs by the reaction sequence $CH_4+H <=> CH_3+H_2$, CH_3+CH_3 $(+M) <=> C_2H_6$ $(+M)$,$C_2H_6+H <=> C_2H_5+H_2$, $C_2H_5(+M) <=>C_2H_4+H(+M)$, $C_2H_4+CH_3<=>C_2H_3+CH_4$, and $C_2H_3(+M)<=>C_2H_2+H(+M)$ in the fuel-rich region as determined by reaction flux analysis. Other minor species detected were C_3H_4, 1,3-butadiene (C_4H_6), vinylacetylene (C_4H_4), diacetylene (C_4H_2), 1,3-hexadien-5-yne (C_6H_6), and cyclopentadiene (C_5H_6). The concentrations for allene and propyne have been reported as a total C_3H_4 mole fraction, due to the overlap of eluting C_3 species from the capillary column. The measured C_3H_4 levels peaked at about 2400 ppm, that is a factor of 10 higher than the model predictions. Calculated C_3H_4 profile also exhibited a two order of magnitude change in concentration at 4 mm from the fuel burner port. This behavior differs substantially from the measured C_3H_4 profile, and directly impacts the behavior of the calculated aromatic and PAH profiles as discussed in the next section. According to the model, C_3H_4 production was primarily driven by methyl addition to acetylene to form propyne and H-atom. It is possible that the use of inappropriate rate parameters, inadequate radiation corrections for the temperature measurements in the fuel rich region of the flame can account for this behavior. The propyne was removed by

isomerization to allene or undergoes H-atom abstraction by methyl to form propargyl and methane. The diacetylene was the most abundant of the C_4 hydrocarbons formed, with the peak concentration of 400 ppmv. Model predictions were a factor of 6 lower, and this can be attributed to the underpredicted acetylene concentrations by the model. The primary diacetylene production pathway was $C_2H_2+C_2H<=>C_4H_2+H$. The experimental peak levels of vinylacetylene and 1,3-butadiene were 111 ppmv and 26 ppmv, respectively. The model predicted the 1,3-butadiene peak concentration fairly well but underpredicted the vinylacetylene levels by an order of magnitude. The cyclopentadiene (c-C_5H_6), the smallest ring compound detected, reached a maximum concentration of 2.6 ppmv, which the model fairly well reproduced. The cyclopentadiene is formed through the oxidation of the phenyl ring by the reaction sequence, $C_6H_5+O_2<=>C_6H_5O+O$, $C_6H_5O<=>c\text{-}C_5H_5+CO$, and $c\text{-}C_5H_5+H<=>c\text{-}C_5H_6$.

Benzene

As shown in Fig. 4, benzene was the most abundant aromatic species produced with a peak concentration of about 90 ppm at 4 mm from the burner nozzle, a level similar to that measured in a lower strain flame [11]. Unfortunately, model predictions were a factor of 40 lower. This, however, is not surprising because benzene formation is closely linked to C_3 species, which as noted before, had some problems. It must also be noted that in our previous premixed flame modeling work [20,31], benzene formation rate from propargyl recombination was calibrated in the 1400-1600 K temperature range. In the present study, benzene formation takes place in the 1000K-1300K temperature range. This difference in temperature ranges could alter the predominant benzene formation mechanism from the sequence, $H_2CCCH+H_2CCCH<=>C_6H_5(Phenyl)+H$, and $C_6H_5+H<=>C_6H_6$, to the $H_2CCCH+H_2CCCH<=>C_6H_6(Benzene)$. Changes in the gas density, mechanism and rate constants would account for the discrepancy between the measured and predicted

benzene concentrations, and suggest further work in this area.

Substituted Benzenes

Toluene, styrene, and phenyl acetylene were the only substituted aromatics detected in this flame as shown in Fig. 4. These species exhibited a fairly broad and flat concentration profile in the fuel-side region, similar to benzene. The calculated toluene concentration also abruptly dropped off near 4.5 mm; this feature, which also common to all the PAH is a subject of current investigation. The measured toluene concentration exhibits a peak concentration of about 2 ppm which is in fair agreement with the predicted maximum of 4.5 ppm. According to the model, toluene was formed primarily by the sequence, $CH_3CCCH_2+H_2CCCH<=>C_6H_5CH_2+H$, and $C_6H_5CH_2+H<=>C_6H_5CH_3$. Interestingly, the model predicted greater toluene abundance than the benzene, a result that is not supported by the experimental data. The measured and predicted peak styrene concentrations were in excellent agreement, with a maximum concentration of ca.1 ppm. The styrene was produced exclusively by the $C_6H_5+C_2H_4<=>C_6H_5C_2H_3+H$ reaction. The phenylacetylene peak concentration was predicted to be 1.6 ppm which is also in fair agreement with the measured value of 5.0 ppm. The phenyl acetylene production is due to ethylene addition to phenyl to form styrene and H-atom, followed by styrene dehydrogenation. The $C_6H_5+C_2H_2<=>C_6H_5C_2H+H$ reaction, which might be expected to produce phenylacetylene, was favored in the reverse direction and served as the primary phenylacetylene removal step.

Polycyclic Aromatic Hydrocarbons

The measured and predicted concentrations of naphthalene, acenaphthylene, phenanthrene, anthracene, pyrene, and fluoranthene are shown in Fig. 5. As evident from this figure, calculated PAH mole fraction profiles shared features similar to C_3, C_4, and aromatics as described above, and that their mole fractions increased dramatically at about 4 mm from the burner port. This result also

is not supported by the experiments. Experimental measurements indicated that naphthalene and pyrene were the first and second most abundant PAH formed respectively in this flame, a result consistent with premixed flames [29]. The model also correctly predicted naphthalene as the dominant polycyclic aromatic formed, but underpredicted the pyrene levels by two orders of magnitude. The latter is a surprising result and the reaction phenanthryl-1 + C_2H_2<=>pyrene + H, using the rate constants obtained from [32] did not contribute significantly to pyrene formation in this flame. The measured acenaphthylene ($C_{12}H_8$) peak concentration in the flame reached 4 ppm. The model was able to predict this peak concentration only to within a factor of ten, although a better agreement was achieved in modeling premixed flames [20]. The failure of the Indenyl + H_2CCCH <=> Acenaphthylene + H reaction step in this study to produce experimentally observed levels of acenaphthylene is due to indenyl's inability to compete against methyl radicals for propargyl radicals in this region of the flame.

The primary route for naphthalene production was through the cyclopentadienyl self-combination step [20], c-C_5H_5+c-C_5H_5<=>$C_{10}H_8$+H+H, where c-C_5H_5 is produced by the sequence C_6H_5+O_2<=>C_6H_5O+O and C_6H_5O<=>c-C_5H_5+CO. The key step in the production of naphthalene as well as other PAH is phenyl oxidation by O_2 as indicated above. Previous work [32] had indicated that if the C_6H_5+O_2 reaction competes effectively with the polymerization process, as represented by C_6H_5+nC_2H_2<=>PAHs, then PAH production would be *inhibited.* Our modeling studies show that the removal of phenyl by O_2 leading to cyclopentadienyl will actually *promote* PAH formation [33].

As seen in Fig.5, the phenanthrene and anthracene levels were well predicted by the model in comparison to the experimental measurements and suggests that the reaction steps used in previous modeling efforts for premixed flames [20,31] are also valid in the opposed flow diffusion flame.

The measured peak concentrations of the isomers with three fused-aromatic rings, phenanthrene and anthracene, were 0.8 ppm and 0.2 ppm respectively. The phenanthrene is formed in greater abundance than its isomer, anthracene, due to the higher thermochemical stability of the former [30]. The model was able to reproduce fairly well the relative abundance of these two species. Reaction rate analysis revealed that production of phenanthrene in this flame occurs via resonantly stabilized benzyl and indenyl radicals via the sequence $C_6H_5CH_2+C_2H_2$<=>Indene+H, Indene+H<=>Indenyl+H_2, and Indenyl+c-C_5H_5<=>Phenanthrene+H+H. The model predicted a relatively small concentration of indene in the flame (maximum concentration of indene and indenyl was less than 0.015 ppm and 1.0 ppm, respectively). These indene levels are below the detection limit of the MS. The reaction, Indenyl+c-C_5H_5<=>Phenanthrene+H+H, represents an analogous process to the cyclopentadienyl combination proposed earlier for the formation of naphthalene in premixed flames [20,31].

The peak anthracene concentration was well reproduced by the model using the Phenanthrene <=> Anthracene isomerization kinetics suggested by Colket and Seery [35]. This reaction also proved successful in modeling the anthracene levels in premixed flames as well [20,31].

The model at hand was unable to correctly predict the concentrations of any polycyclics that had a shared C_5 structure fused (i.e. fluoranthene) to any other aromatic rings, and clearly suggests further work in this area.

In conclusion, the GC/MS analysis of gases withdrawn from opposed jet diffusion flames of methane indicate a rich chemistry with the formation of a large number of aromatics, PAH that were also seen in fuel rich premixed flames. Detailed kinetic analysis of this flame structure revealed that our understanding of the underlying chemical kinetics of fuel-rich combustion of CH_4 is in place to make reasonable predictions. Nevertheless, several issues need to be resolved to make these

predictions quantitative. Most significantly, the discrepancy between model predictions and the experiment for C_3 and C_4 products needs to be closed. Similar discrepancies also exist for aromatics and PAH and require further studies..

Acknowledgments

This research was supported, in part, by the US Environmental Protection Agency Grant No:R819178-01, the National Science Foundation CTS-9311848, the UCLA Center for Clean Technologies, and the Petroleum Environmental Research Forum Project 92-19. The chemical kinetic modeling portion of this work was carried out under the auspices of the U. S. Department of Energy by the Lawrence Livermore National Laboratory under contract No. W-7405-ENG-48.

References

1. Clean Air Act Amendments; Public Law 101-549, 1990.

2. Klaassen, C.D., Amdur, M.O., and Doull, J. Casaret and Doull's Toxicology, 2nd. Ed., Macmillian , NY.

3. Hansell, D.W., England, G.C., Soelberg, N.,Seeker, W.R., Lev-on,M.,Folkarkow, S., Paper Air & Waste Management Association 85th Annual Meeting, Kansas City, Missouri,1992.

4. Clement Associates Inc., US EPA, 1991, Integrated Risk Information System (IRIS).

5. Du, D.X., Axelbaum, R.L., and Law, C.K., *Twenty Second Symposium (International) on Combustion*, The Combustion Institute,Pittsburgh, 1988, pp. 387-

6. Drake, M.C., " Kinetics of Nitric Oxide Formation in Laminar and Turbulent Methane Combustion", GRI-85/0271, Gas Research Institute, 1985.

7. Chelliah, H.K., Law, C.K., Ueda, T., Smooke, M.D., and Williams, F.A., *Twenty Third Symposium (International) on Combustion*, The Combustion Institute, Pittsburgh, 1990, pp. 503-511.

8. Tsuji, H., and Yamaoka, I., *Twelfth Symposium (International) on Combustion*, The Combustion Institute, Pittsburgh, 1969 pp. 997-1005.

9. Dixon-Lewis, G., David, T., Gaskell, P.H., Fukutani, S., Jinno, H., Miller, J.A., Kee, R.J., Smooke , M.D., Peters, N., Effelsberg, Warnatz, J., and Behrendt, F., *Twentieth Symposium (International) on Combustion*, The Combustion Institute, Pittsburgh, 1984, pp. 1893-1904.

10. Kee, R.J., Miller, J.A., Evans, G.H., and Dixon-Lewis, G., *Twenty Second Symposium (International) on Combustion*, The Combustion Institute, Pittsburgh, 1988, pp. 1479.

11. Zhang, C, Atreya, A., and Lee, K., *Twenty Fourth Symposium (International) on Combustion*, The Combustion Institute, Pittsburgh, 1992, pp. 1049-1057.

12 Puri, I., and Seshardi, K., Combust. Flame 65:137-150 (1986).

13. Fitch, W.L., and Sauter, A.D., Anal. Chem. 55: 832-836 (1983).

14. Lutz, A. E., Kee, R. J. , and Grcar, J. R. OPPDIF: A FORTRAN Program for Computing Opposed-Flow Diffusion Flames, Sandia National Laboratories Report No. SAND95-XXXX, September, 1995.

15. Kee, R.J., Rupley, F.M., and Miller, J.A., The Chemkin Thermodynamic DataBase, Sandia Report #SAND87-8215B (1987).

16. Burcat, A., and McBride, B., 1994 Ideal Gas Thermodynamic Data for Combustion and Air-Pollution Use, Technion Report #TAE 697 (1993).

17. Stein, S.E., and Fahr, A., J. Phys. Chem., 89:3714-3725 (1985).

18. Stein, S.E., and Brown, R.L., J. Am. Chem. Soc., 113:787-793 (1991).

19. Benson, S.W., (1976), Thermochemical Kinetics, Second Edition, John Wiley and Sons.

20. Marinov, N.M., Pitz, W.J., Westbrook, C.K., Castaldi, M.J., and Senkan, S.M.: Comb. Sci. and Tech., in press 1996.

21. Kee, R.J., Dixon-Lewis, G., Warnatz, J., Coltrin, M.E., and Miller, J.A., The Chemkin Transport Database, Sandia Report #SAND86-8246 (1986).

22. Wang, H., and Frenklach, M., Combust. Flame, 96:163-170 (1994).

23. Miller, J.A., and Melius, C.F., Combust. Flame, 91: 21-39 (1992).

24. Tsang, W., J. Phys. Chem. Ref. Data, 17(2): 887-951 (1988).

25. Tsang, W., J. Phys. Chem. Ref. Data, 20(2): 221-273 (1991).

26. Pitz, W.J., Westbrook, C.K., and Leppard, W.K., SAE Transactions, SAE Paper No. 912315 (1991).

27. Emdee, J., Brezinsky, K., and Glassman, I., J. Phys. Chem., 96:2151-2161 (1992).

28. Tsuji, H., and Yamaoka, I., *Thirteenth Symposium (International) on Combustion*, The Combustion Institute, Pittsburgh, 1971 pp. 723-731.

29. Castaldi, M., Vincitore, A.M.,and Senkan, S.M., Combust. Sci. Tech.107:1-19 (1995).

30. Frenklach, M., and Warnatz,J., Combust. Sci. Tech. 51: 265 (1987).

31. Castaldi, M. J, Marinov, N.M., Melius, C. F., Huang, J., Senkan, S.M. Pitz, W.J., and Westbrook, C.K., Experimental and Modeling Investigation of Aromatic and Polycyclic Aromatic Hydrocarbon Formation in a Premixed Ethylene Flame, submitted for publication,1996.

32. Wang, H., and Frenklach, M., J. Phys. Chem., 98:11465-11489 (1994).

33. Glassman, I., Combustion, Second Edition, Academic Press, New York, 1986.

34. Melius, C.F., Colvin, M.E., Marinov, N.M., Pitz, W.J., and Senkan, S.M.: Twenty-Sixth Symposium (International) on Combustion, The Combustion Institute, Pittsburgh, 1996, Submitted.

35. Colket, M.B., and Seery, D.J., Twenty-Fifth Symposium (International) on Combustion, The Combustion Institute, Pittsburgh, 1994, pp. 883-891.

36. Cox, J.D.,and Pilcher, G., Thermochemistry of Organic and Organometalic Compounds, Academic Press, London, 1970.

Table 1. Experimental Conditions of a Methane, Opposed Flow, Diffusion Flame

Oxidizer Burner Outlet Velocity [a], v_O, cm/s	16.12
Fuel Burner Outlet Velocity [a], v_F, cm/s	13.16
Inlet Oxidizer Stream Density [a], g/L	1.569
Inlet Fuel Stream Density [a], g/L	0.9
Computed Strain Rate, sec^{-1}	35
Computed Stoichiometric Mixture Fraction, Z_{st}	0.06
Oxidizer Composition, x_{O2}	0.2
Fuel Composition, x_F	0.75
Burner Jet Separation, L, mm	15
Fuel Stream Carbon Density [a], g carbon/cc flow	3.68×10^{-4}

a. Values calculated at 298 K, and 1 atm.

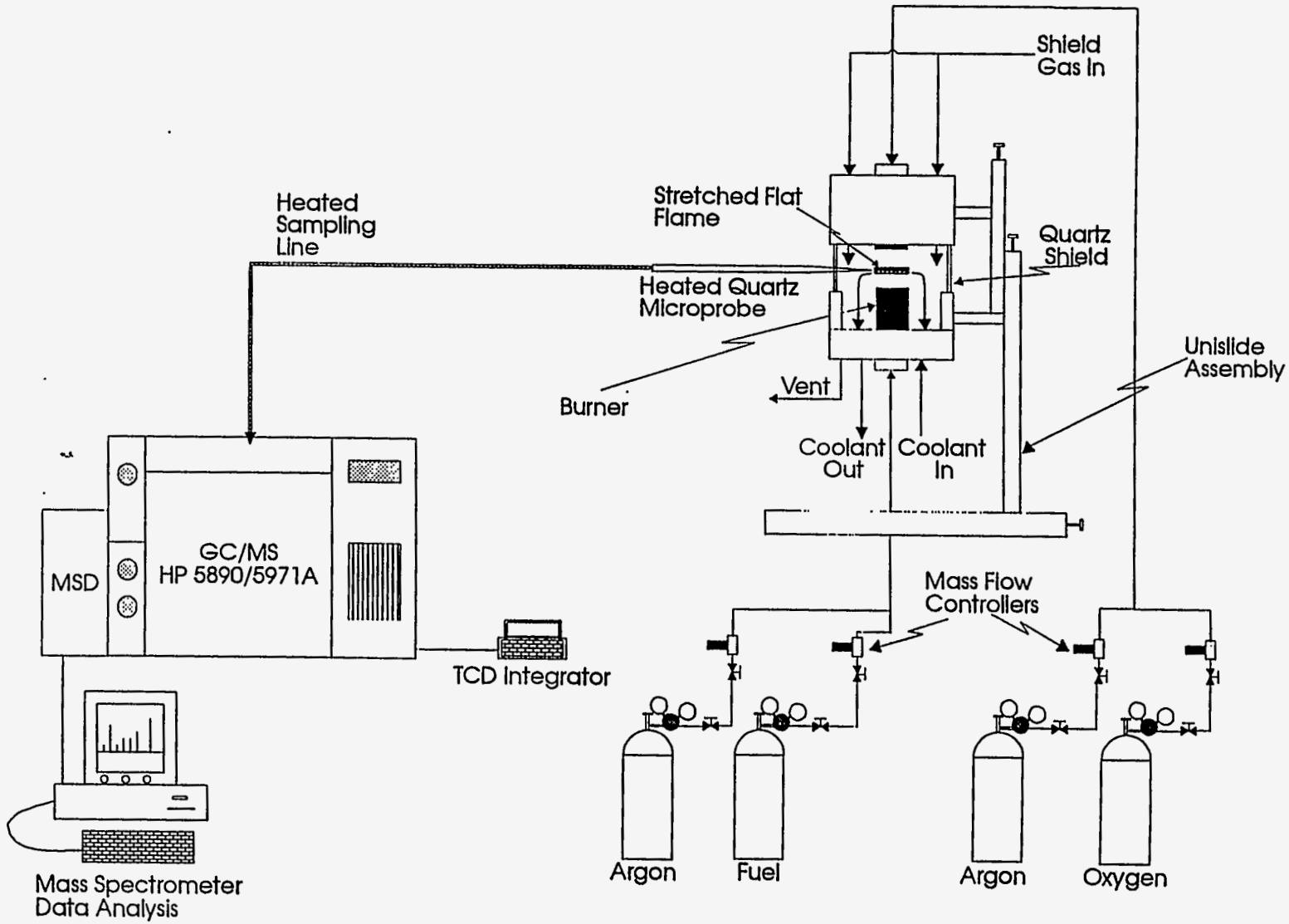

Fig. 1. An illustration of the experimental burner and sampling probe configuration.

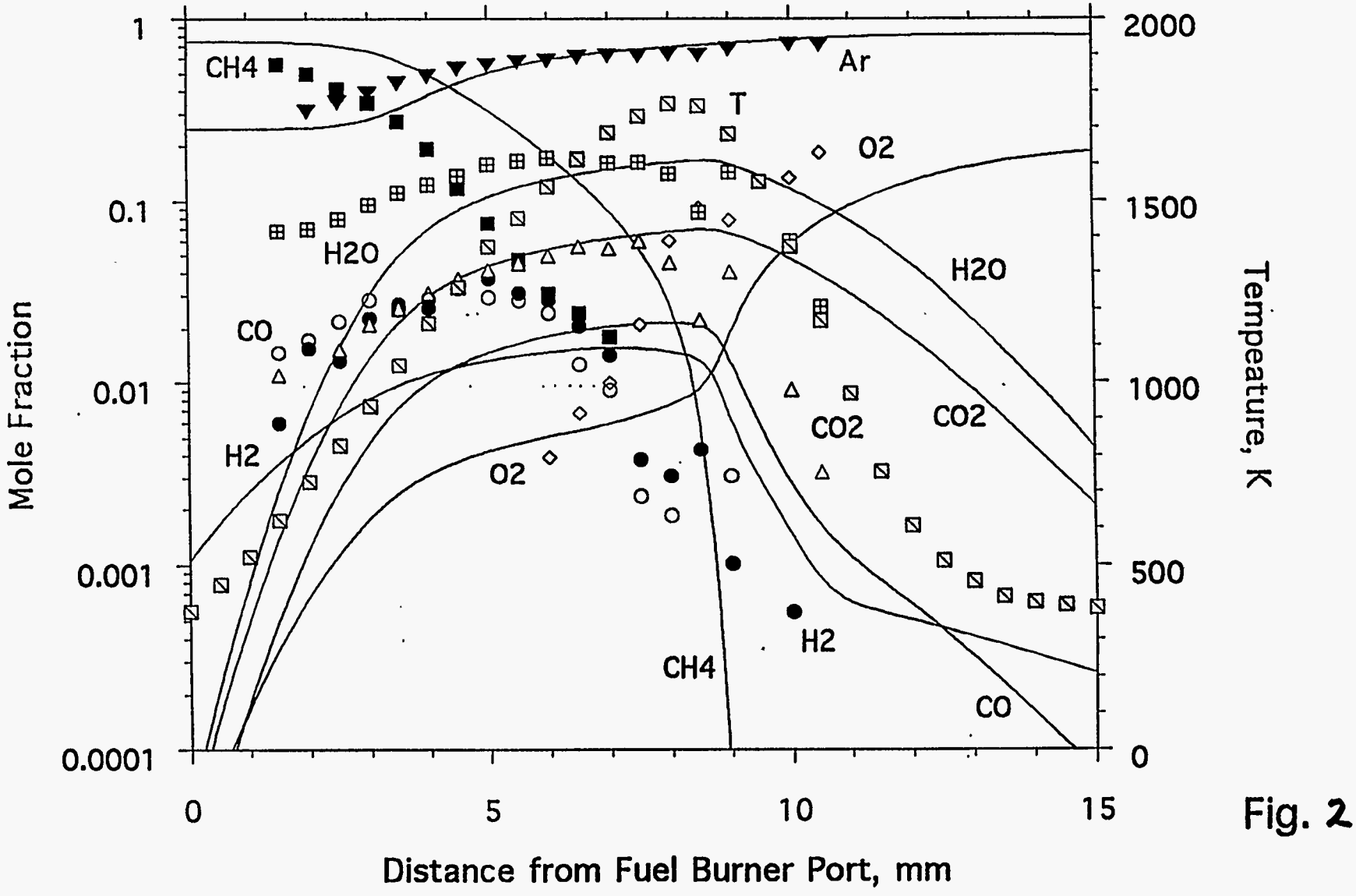

Fig. 2

Fig. 2. Measured and calculated profiles of major species and temperature along the center of the flame.

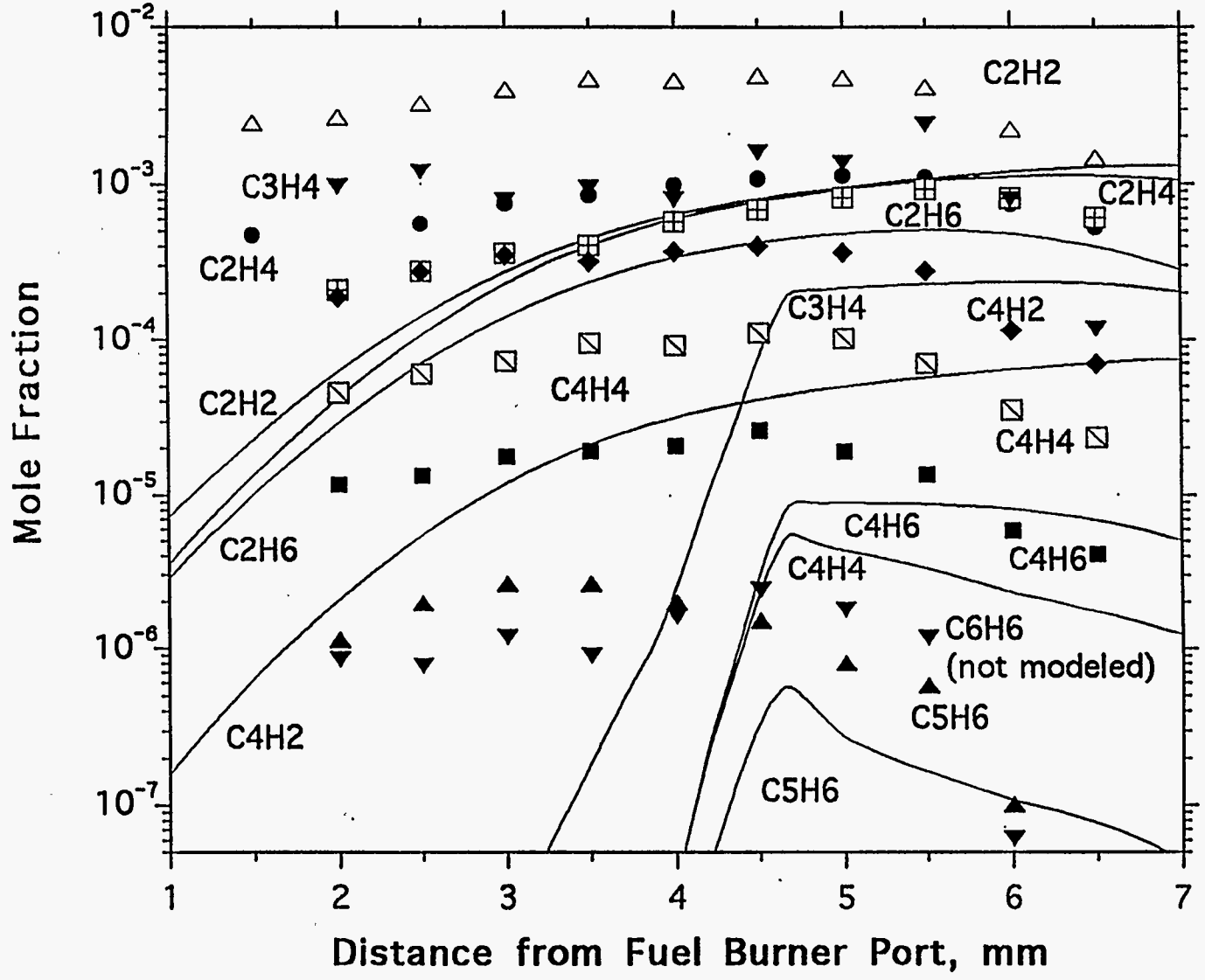

Fig. 3

Fig.3. Measured and calculated profiles of minor species along the center of the flame.

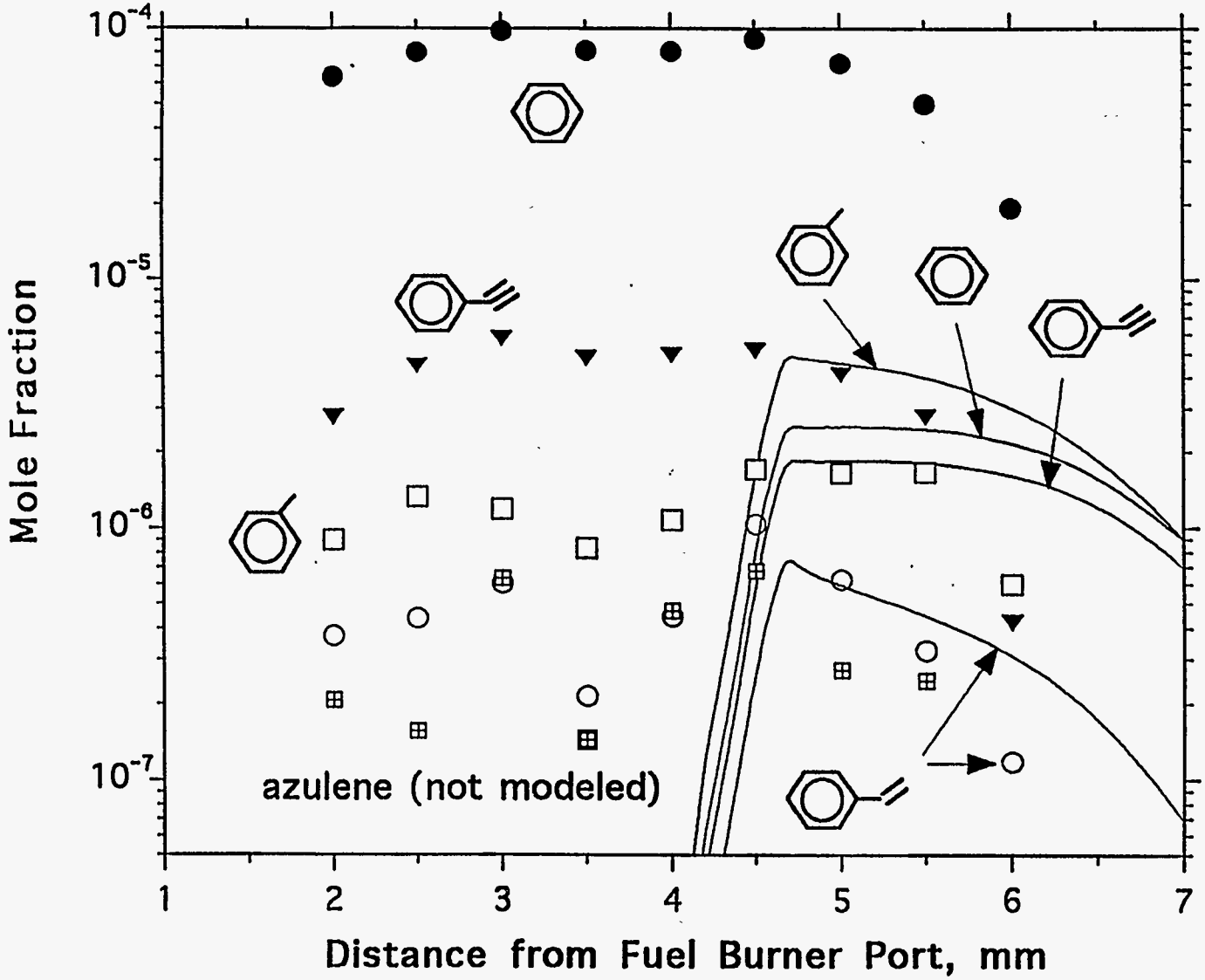

Fig. 4. Measured and calculated profiles of aromatic and substituted aromatic species along the center of the flame.

Fig. 4

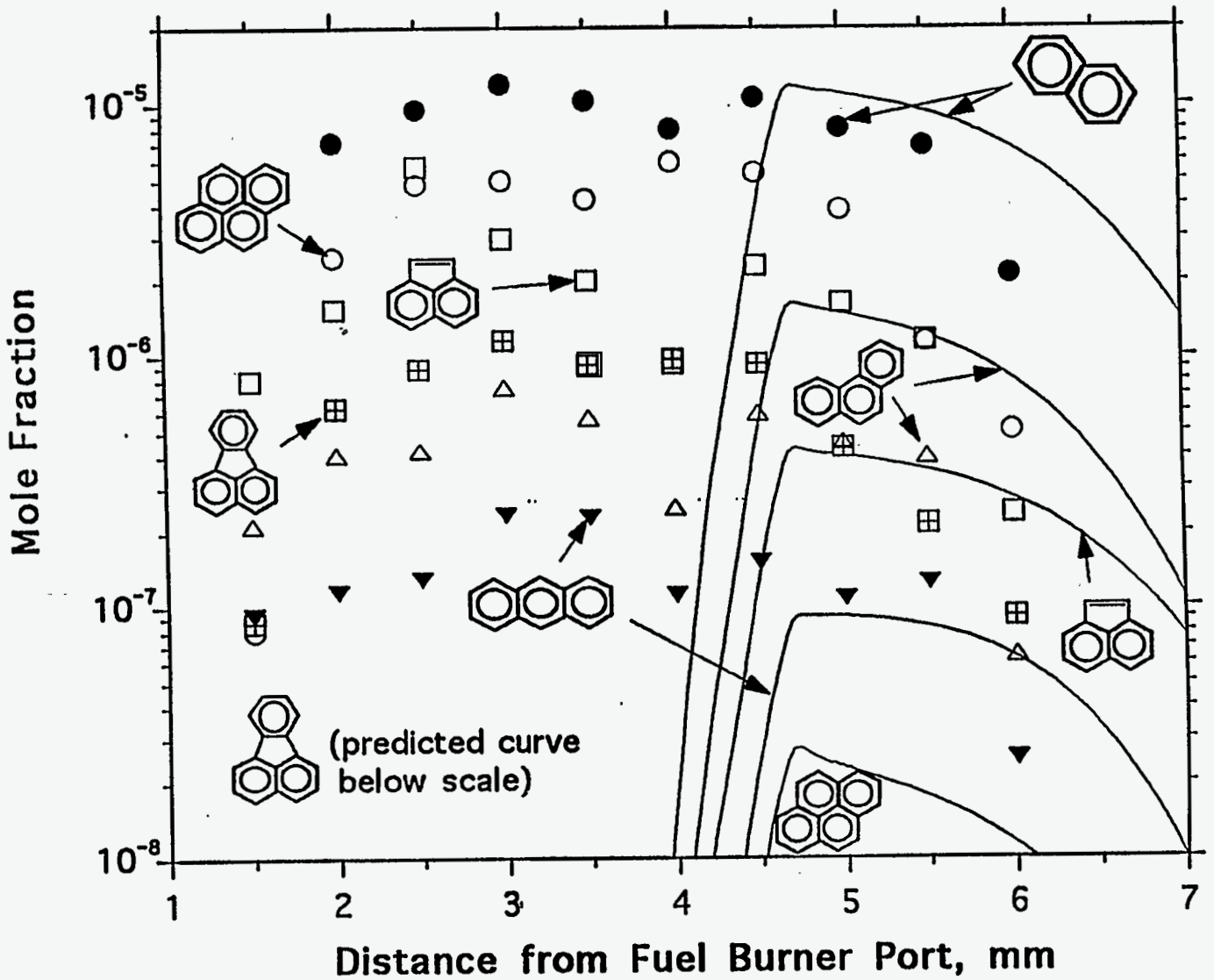

Fig. 5. Measured and calculated profiles of trace PAH species along the center of the flame.

Fig. 5